Translational Oncology 15 (2022) 101272

Contents lists available at ScienceDirect

Translational Oncology

journal homepage: www.elsevier.com/locate/tranon

Original Research

BX-795 inhibits neuroblastoma growth and enhances sensitivity towards chemotherapy

Rameswari Chilamakuri [a], Danielle C. Rouse [a], Yang Yu [b], Abbas S. Kabir [a], Aaron Muth [a], Jianhua Yang [b], Jeffery M. Lipton [c], Saurabh Agarwal [a,*]

[a] Department of Pharmaceutical Sciences, College of Pharmacy and Health Sciences, St. John's University, New York, NY, USA
[b] Texas Children's Cancer Center, Department of Pediatrics, Baylor College of Medicine, Houston, TX, USA
[c] Institute of Molecular Medicine, Feinstein Institutes for Medical Research, New York, NY, USA

ARTICLE INFO

Keywords:
PDK1
BX-795
Neuroblastoma
Pediatric cancer
AKT pathway
Drug repurposing
Drug synergy

ABSTRACT

High-risk neuroblastoma (NB) represents a major clinical challenge in pediatric oncology due to relapse of metastatic, drug-resistant disease, and treatment-related toxicities. An analysis of 1235 primary NB patient dataset revealed significant increase in *AKT1* and *AKT2* gene expression with cancer stage progression. Additionally, Both *AKT1* and *AKT2* expression inversely correlate with poor overall survival of NB patients. *AKT1* and *AKT2* genes code for AKT that drive a major oncogenic cell signaling pathway known in many cancers, including NB. To inhibit AKT pathway, we repurposed an antiviral inhibitor BX-795 that inhibits PDK1, an upstream activator of AKT. BX-795 potently inhibits NB cell proliferation and colony growth in a dose-dependent manner. BX-795 significantly enhances apoptosis and blocks cell cycle progression at mitosis phase in NB. Additionally, BX-795 potently inhibits tumor formation and growth in a NB spheroid tumor model. We further tested dual therapeutic approaches by combining BX-795 with either doxorubicin or crizotinib and found synergistic and significant inhibition of NB growth, in contrast to either drug alone. Overall, our data demonstrate that BX-795 inhibits AKT pathway to inhibit NB growth, and combining BX-795 with current therapies is an effective and clinically tractable therapeutic approach for NB.

Introduction

Neuroblastoma is the most common extra-cranial solid pediatric tumor that develops during early embryonic stages, and accounts for almost 15% of pediatric cancer-related deaths [1]. Despite major advancements in therapeutic regimens of dose-intensive chemotherapies, the overall 5 year survival rate for high-risk neuroblastoma (NB) patients is still less than 50% [2]. Current therapies for managing NB are highly toxic, have significant long-term side effects, and are associated with an increased risk of developing secondary malignancies. Therefore, developing targeted therapeutic approaches by identifying the genetic factors and molecular pathways involved in driving NB pathogenesis is critical.

The phosphoinositide-3 kinase (PI3K)/AKT pathway is a major intracellular signaling pathway that is known to regulate cell growth, proliferation, and metabolism [3]. PI3K acts as a signal transducer which phosphorylates and activates phosphatidyl-inositol 4,5-biphosphate (PIP2), which in turn generates phosphatidyl-inositol 3–5-triphosphate (PIP3), a reaction that is negatively regulated by PTEN [4]. PIP3 then translocate AKT and PDK1 (3-Phosphoinositide--dependent kinase 1) from the cytoplasm to the plasma membrane, where PDK1 phosphorylates AKT at T308 to activate it [5]. Further activation of AKT is mediated by mTORC2, which phosphorylates S473 of AKT [6]. Genetic mutations or amplification of AKT have been reported in multiple adult cancers such as lung, breast, endometrial, pancreatic, and melanoma [7–10]. In NB, AKT mutations have not been reported, however, abnormal AKT activation is shown to be correlated with an overall poor NB prognosis [11]. Studies have shown that directly inhibiting AKT in turn inhibits NB pathogenesis and progression [12, 13].

PDK1 is essential for the activation of AKT as well as other important regulators, including p70 ribosomal S6-kinase (S6K), TSC2, and GSK3β [14]. These regulators also control several well-studied cancer drivers, such as FOXO3a, BAD, MDM2, and MYCN [15,16]. Among these, MYCN is a key genetic biomarker for NB risk stratification, and is a known driver of NB oncogenesis and disease progression. This establishes PDK1

* Corresponding author at: St John's University, Pharmaceutical Sciences, St. Albert's Hall, Suite B-65, 8000 Utopia Parkway, New York, NY, United States.
E-mail address: agarwals@stjohns.edu (S. Agarwal).

https://doi.org/10.1016/j.tranon.2021.101272
Received 27 July 2021; Received in revised form 20 October 2021; Accepted 26 October 2021

as a central regulator of multiple signaling pathways which regulate cancer growth, metabolism, apoptosis, and drug-resistance [17]. Aberrant levels of activated PDK1 leads to increased AKT levels, and is reported in multiple cancer types, including melanoma, breast, lung, gastric, prostate, hematological, and ovarian cancers [18–20]. Therefore, directly targeting PDK1 activation to inhibit AKT and other oncogenic pathways holds strong therapeutic rational for targeted cancer therapy [21]. BX-795 is a potent ATP-competitive small molecule inhibitor of PDK1 and TANK-binding kinase 1 (TBK1) [22–24]. BX-795 has been reported as an anti-viral drug for treating the herpes simplex virus infection [25,26], reducing inflammation [27], and as an effective therapeutic approach in multiple cancer types, such as oral squamous cell carcinoma [28], bladder cancer [29,30], pancreatic ductal adenocarcinoma [31], breast cancer [32], and hepatocellular carcinoma [33].

Anaplastic lymphoma kinase (ALK) is a major clinical target, characterized by chromosomal translocation in which the ALK kinase domain is fused to a vast number of amino-terminal partners [34]. Around 5–8% of NB patients exhibit ALK mutations in one of three hotspot residues in the tyrosine kinase domain amino acids, F1174, F1245, and R1275. R1275 is the most common ALK mutation exhibited in ~43% of ALK mutant tumors, followed by F1174 in 30% and F1242 in 12% of ALK mutant tumors [35]. R1275Q, F1174L, and F1245C dominant mutations promotes NB cell proliferation, activation of downstream signaling pathways, and growth factor independence [36,37]. Crizotinib is a first generation multitarget tyrosine kinase inhibitor that directly inhibits the kinase activity of ALK, and indirectly suppresses the c-Met and ROS1 [38,39]. Crizotinib is FDA approved for the treatment of ALK positive advanced non-small cell lung cancer [38], and is currently under clinical trials for the treatment of lobular breast carcinoma, gastric cancer, triple negative breast cancer, hematologic metastatic cancers, and NB.

In the present study, we investigated the effects of BX-795 on NB growth. Our study demonstrates that BX-795 specifically inhibits PDK1 activation, thereby inhibiting AKT phosphorylation and activation. BX-795 was observed to significantly inhibits NB cell proliferation, inhibits colony and 3D spheroid formation, induces apoptosis, blocks cell cycle progression, and sensitizes NB to doxorubicin and crizotinib. Overall, this study indicates; (1) the role of PDK1 as a therapeutic target in NB, (2) BX-795 is a potent inhibitor of NB growth, and (3) combining BX-795 with current therapies is a novel, less toxic, and more effective therapeutic strategy for NB.

Materials and methods

Cell culture and reagents

Human neuroblastoma cell lines, both MYCN non-amplified (SH-SY5Y, SK-N-AS, CHLA-255) and MYCN-amplified (NGP, LAN5, CHLA-255-MYCN), were routinely cultured and maintained as described previously [40]. CHLA-255 and CHLA-255-MYCN cell lines were courtesy provided by Dr. Leonid Metelitsa of Baylor College of Medicine, Houston [41]. Control fibroblast cell lines WI-38, NIH-3T3, and COS-7 were obtained from ATCC. Briefly, all NB cell lines were cultured in RPMI-1640, NIH-3T3 and COS-7 cell lines were cultured in DMEM, and WI-38 cell line was cultured in EMEM media, supplemented with 10% FBS, 1% penicillin/streptomycin, and 1% L-glutamine. All cell lines were validated via short-tandem repeat analysis for genotyping within the past 6 months and routinely tested for Mycoplasma monthly. Primary antibodies anti-PDK1(3062S), anti-pPDK1 (Ser241; 3438S), anti-AKT (9272S), anti-pAKT (Thr308; 9275S), anti-p70 S6 kinase (S6K; 9202S), anti-p-p70 S6 kinase (pS6K; Thr389; 9205S), anti-cyclophilin B (43603S), and anti-rabbit IgG HRP-linked secondary antibody (7074S) were purchased from Cell Signaling Technology. BX-795, crizotinib, and doxorubicin were purchased from MedChemExpress, NJ.

Clinical patient dataset

The patient datasets including a total of 1235 primary NB patients were analyzed, including the Versteeg dataset ($N = 88$), Kocak dataset ($N = 649$), and SEQC dataset ($N = 498$). These datasets contain microarray profiles of unique primary tumors and is publicly available in the R2: Genomic Analysis and Visualization Platform. This platform also supports multi-parametric analysis of NB patient outcomes with gene expression.

Cell viability and clonogenic assay

Cell viability assays were performed using the CellTiter 96 AQueous One Solution Cell Proliferation Assay (G3582; Promega) according to the manufacturer's instructions and as described previously [41,42]. Briefly, 1×10^4 cells per well were added into 96-well plates and treated with various concentrations of indicated drugs for 72 h. The drug treated plates were then incubated and analyzed by spectrophotometric absorbance at 490 nm using a microplate reader (SpectraMax iD3, Molecular Device). The data was analyzed and IC_{50} values were calculated using GraphPad Prism 8 software. Clonogenic assays were performed using standard conditions as previously described [43]. Briefly, 1×10^2 NB cells were seeded per well into 6-well plates, followed by treatment with the indicated drug concentrations. After 48 h, fresh media was added, and plates were incubated for 10–12 days. Colonies were stained by adding a 0.2% crystal violet solution and visualized and counted using ChemiDoc (BioRad; ChemiDoc XRS+). All assays were performed in triplicate and repeated at least three times with appropriate controls.

Apoptosis and cell cycle assay

Apoptosis in NB cell lines was analyzed using the Muse Annexin V & Dead Cell Kit (MCH100105; Luminex Corp) according to the manufacturer's instructions. Briefly, NB cells were treated with the indicated doses of BX-795 for 16 h, followed by washing with cold PBS and incubation with 100 μl of the kit reagent for 20 min. Similarly, cell cycle analysis in NB cells was performed using the Muse Cell Cycle Kit and reagent (MCH100106; Luminex Corp) according to the manufacturer's instructions. The samples were analyzed using the Guava Muse cell analyzer (Luminex Corp).

Spheroid assays

3D spheroid assays for NB were performed using round bottom 3D spheroid 96-well plates (4515; Corning) according to the manufacturer's instructions. NB cells were seeded at 1×10^3 cells/well and incubated for 3 days to develop spheroids of about 300 μm in size. Wells that have at least 300 μm size spheroids were selected and randomized for treatment with the indicated drug doses. Treatment continued for 7–10 days with regular replenishment of the drugs every three days. Spheroid images were captured regularly using Leica DMi1 microscope, and spheroid size and volume was determined using the LASX software suite (Leica Microsystems). After terminal imaging, the viability of the spheroid cells was measured using the Viability/Cytotoxicity Assay Kit for Animal Live & Dead Cells (3002; Biotium Inc.) according to the manufacturer's instructions. The assay kit contains Calcein AM dye that stains live cells and yields green fluorescence, as well as an Ethidium homodimer III dye that stains dead cells and yields red fluorescence. The stained spheroids were imaged and analyzed using the EVOS FL imaging system (Thermo Scientific). Furthermore, the fluorescence was quantified using a microplate reader (SpectraMax iD3, Molecular Device) at 517 nm for the Calcein AM dye and at 625 nm for the EthD-III dye. Additionally, the 3D spheroid viability was determined using the CellTiter-Glo 3D Cell Viability Assay (G968; Promega) according to the manufacturer's instructions. Briefly, the spheroids were homogenized in the presence of the dye reagent and incubated for 30 min followed by

quantifying the luminescence using a multi-mode microplate reader (SpectraMax iD3, Molecular Device).

RNA extraction and quantitative real time RT-PCR

Total RNA was extracted from NB cells by using a RNeasy plus mini kit (74,134; Qiagen), according to the manufacturer's instructions. RNA was reverse transcribed into cDNA using the high-capacity cDNA reverse transcription kit (4,368,814; Applied Biosciences) as per the manufacturer's protocol. Prepared cDNA was used in RT-PCR reactions for individual genes (Supplementary Table 1) in triplicate using the SYBR Green master mix (4,385,610; ThermoFisher Scientific) on a QuantStudio 3 Real Time PCR System (ThermoFisher Scientific). The relative expression was normalized by using GAPDH as a housekeeping gene. The *p*-values were calculated by Student's *t*-test to determine the expression-fold difference of individual genes.

Immunoblotting assays

Immunoblotting assays were performed as previously described [44]. Briefly, total and phospho-proteins were extracted by lysing cells in RIPA extraction and lysis buffer (89,900; ThermoFisher Scientific) supplemented with protease inhibitor cocktail (Complete mini EDTA free, Roche) and phosphatase inhibitor cocktail (PhosSTOP, Roche). Cell lysates were collected after centrifuging for 15 min at 13,000 rpm followed by protein quantification using the Bradford assay according to the manufacturer's instructions (5,000,205; Bio-Rad). Equal amounts of protein samples were separated on 4–12% SDS-PAGE gels, transferred to PVDF membrane (Bio-Rad), blocked with 5% BSA solution, and probed with the indicated primary antibody overnight at 4 °C. The membrane was then washed and incubated with either anti-mouse or anti-rabbit IgG HRP-conjugated secondary antibody for 2 h at room temperature. Blots were developed using the Clarity ECL Western substrate (Bio-Rad), visualized, imaged, and documented using the ChemiDoc XRS Plus system (Bio-Rad).

Drug synergy studies

Cells were seeded in 96-well plates and combination index (CI) studies were performed by treating cells with either BX-795, doxorubicin, crizotinib alone or BX-795 in combination with doxorubicin or crizotinib in a specific ratio. Cytotoxicity assays were performed as described above followed by calculation of the CI values and dose-reduction indices (DRIs) by using the Chou-Talalay method for drug interactions using CalcuSyn software for the different fractions affected [45]. Equipotent molar ratios of 64:1 between BX-795 and doxorubicin and 58:1 between BX-795 and crizotinib were used. CI <1, $=1$, and >1 indicates synergism, additive effect, and antagonism, respectively. DRI >1, and <1 indicates a favorable and an unfavorable dose-reduction, respectively.

Statistical analysis

In the present study, assays were performed with at least three technical replicates, experiments were repeated at least thrice, and representative results are presented. All values are presented as mean ± standard deviation (SD). A two-tailed Student's *t*-test were used to determine the statistical significance among drug treatment groups. $P < 0.05$ was considered statistically significant. IC_{50} values were calculated with GraphPad Prism 8 software. Patient survival analyses were performed using the Kaplan-Meier method and two-sided log-rank tests.

Results

AKT expression strongly correlates with poor NB prognosis

We investigated the correlation of *AKT1* and *AKT2* expression levels with overall and eventfree NB patient outcome by analyzing primary *NB* patient ($N = 1235$) clinical datasets. Kaplan-Meier survival analysis revealed that expression of both *AKT1* and *AKT2* is inversely correlated with overall and eventfree survival of *NB* patients (Fig. 1, Supplementary Fig. S1). Low expression of both AKT1 and AKT2 showed significantly better prognosis and overall survival (Kocak $N = 649$, AKT1 $p = 5.1e\text{-}07$, AKT2 $p = 2.1e\text{-}06$; SEQC $N = 498$, AKT1 $p = 4.8e\text{-}09$, AKT2 $p = 3.4e\text{-}06$; Versteeg $N = 88$, AKT1 $p = 0.236$, AKT2 $p = 0.236$; Fig. 1A–C, Supplementary Fig. S1 A–C), and also eventfree survival (Kocak, AKT1 $p = 1.2e\text{-}05$, AKT2 p=.8e-09; SEQC, AKT1 $p = 0.069$, AKT2 $p = 8.7e\text{-}07$; Versteeg, AKT1 $p = 0.304$, AKT2 $p = 0.012$; Fig. 1D–F, Supplementary Fig. S1 D–F) in all the patient datasets analyzed. Additionally, aggressive and higher stage NB tumors showed significantly higher AKT1 and AKT2 expression levels (Fig. 2), suggesting that AKT plays a significant role in NB progression. Further, we observed higher expression of AKT1 and AKT2 in MYCN-amplified NB tumors, with a correlation to disease relapse (data not shown). These findings suggest that AKT is a critical prognostic factor for NB patients, and higher expression of AKT leads to poor survival of NB patients.

BX-795 inhibits NB proliferation

To determine the effects of inhibiting AKT activation in NB, we utilized an anti-viral small molecule inhibitor, BX-795. We performed cytotoxicity assays using BX-795 in 6 different NB cell lines that include MYCN amplified (MA) cell lines NGP, LAN-5, CHLA-255-MYCN and MYCN non-amplified (MNA) cell lines SH-SY5Y, CHLA-255, SK-N-AS. These cell lines were selected to represent different NB genetic backgrounds including MYCN status and ALK mutations. Among these NB cell lines SH-SY5Y have ALK F1174L mutation while LAN-5 have ALK R1275Q mutation. To determine that BX-795 selectively inhibits cancer cell growth, we also performed cytotoxicity assays on three control fibroblast cell lines including WI-38, NIH-3T3, and COS-7 (Fig. 3A). Results of the cytotoxicity assays clearly demonstrated the selectivity and potency of BX-795 to inhibit NB cell proliferation in both MYCN-amplified (Fig. 3B) and non-amplified cell lines (Fig. 3C) in a dose-dependent manner and irrespective of ALK mutation status. The IC50 values among different cell lines range from 1.18 μM for NGP to 1.82 μM for SK-N-AS (Fig. 3D). BX-795 showed no to minimal effect on all control fibroblast cell lines tested (Fig. 3A, D). To further validate the anti-proliferative effect of BX-795, we performed clonogenic assays using SH-SY5Y cell line and found that BX-795 significantly reduced the overall NB colony formation capacity in treatment groups in contrast to the control group, in a dose-dependent manner (Fig. 3E, F). These data indicate that BX-795 significantly inhibits NB proliferation and induces cytotoxicity.

BX-795 induces apoptosis and blocks cell cycle progression in NB

To further investigate the mechanism by which BX-795 induces cytotoxicity and inhibits NB proliferation, we performed apoptosis and cell cycle assays in NB cells. Results of Annexin V apoptosis assays in both NGP and SH-SY5Y cell lines clearly demonstrate the efficacy of BX-795 in inducing apoptosis in a dose-dependent manner (Fig. 4A, B). Specifically, 1 μM BX-795 treatment increased the percentage of early apoptotic cells in NGP and SH-SY5Y by 1.5- and 3.5-folds, respectively, in contrast to control tretamnets (Fig. 4A, B). Furthermore, we observed that 1 μM BX-795 treatment significantly inhibits NB cell cycle progression by inhibiting the G2/M transition (Fig. 4C). In response BX-795 treatment, the percentage of cells in the G2/M phase increased by 4.8-fold, while the percentage of cells in the G0/G1 phase decreased by

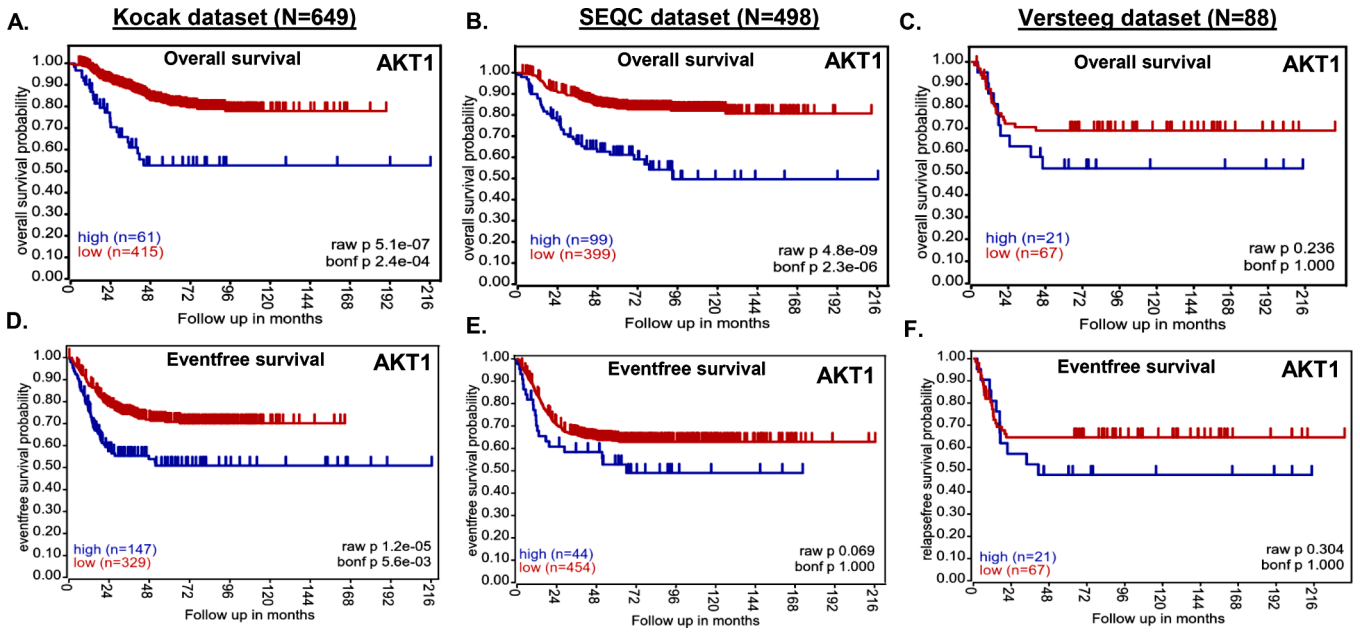

Fig. 1. *AKT expression correlates with poor overall and eventfree survival of NB patients*. Kaplan-Meier analysis in response to AKT1 gene expression showing overall and eventfree survival probability of NB patients. (**A and D)** Kocak dataset of 649 patients. **(B and E)** SEQC dataset of 498 patients. (**C and F)** Versteeg dataset of 88 patients.

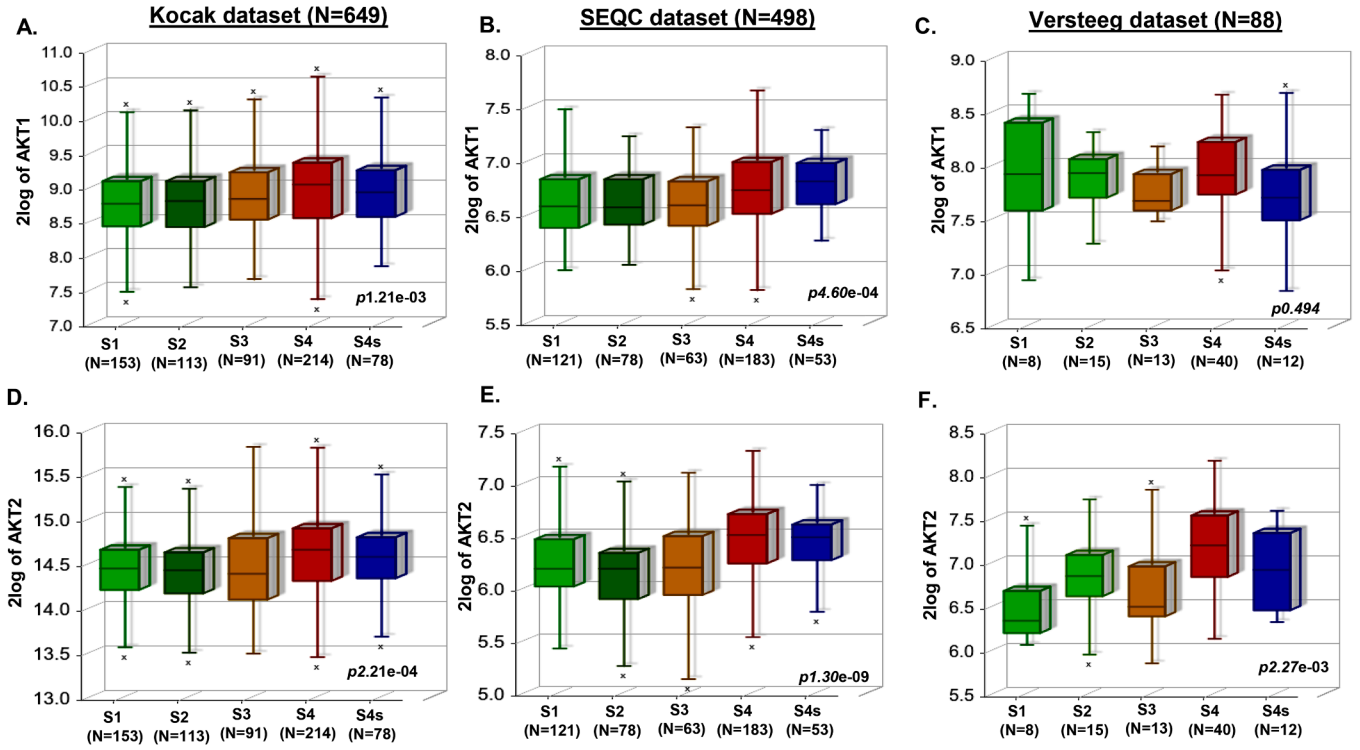

Fig. 2. *AKT expression correlates with NB progression*. Box-plot correlation analysis of NB stages as defined by International Neuroblastoma Staging System (INSS) in response to AKT1 and AKT2 gene expression. (**A and D)** Kocak dataset of 649 patients. **(B and E)** SEQC dataset of 498 patients. (**C and F)** Versteeg dataset of 88 patients.

2.5-fold, in comparison controls (Fig. 4C). This data further indicates the potency of BX-795 in inhibiting NB growth by arresting cell cycle progression and inducing apoptosis.

BX-795 inhibits NB spheroid tumor growth

The results from our 2D or monolayer cell viability studies demonstrated the potency of BX-795 against NB. We then developed 3D-spheroidal tumor models of NB that mimic the physiological growth patterns of *in vivo* tumors. We used SH-SY5Y cell line to develop 3D-spheroid

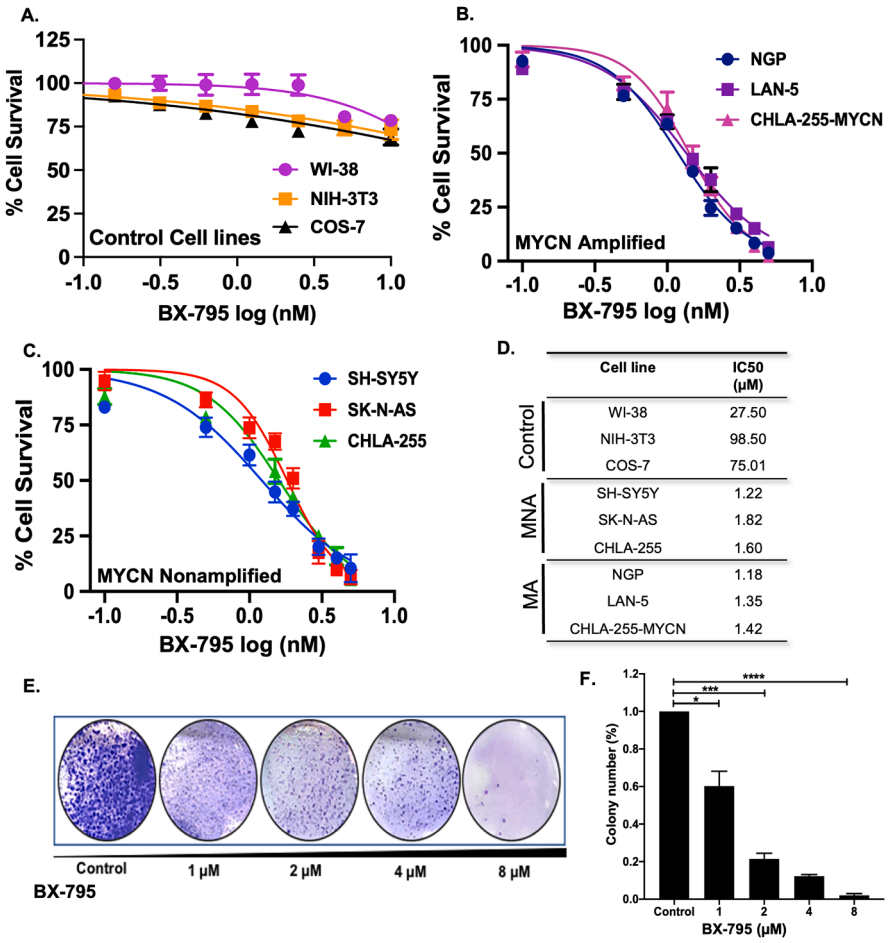

	Cell line	IC50 (μM)
Control	WI-38	27.50
	NIH-3T3	98.50
	COS-7	75.01
MNA	SH-SY5Y	1.22
	SK-N-AS	1.82
	CHLA-255	1.60
MA	NGP	1.18
	LAN-5	1.35
	CHLA-255-MYCN	1.42

Fig. 3. *BX-795 Inhibits NB proliferation*. **(A–D)** Cell cytotoxicity assays in response to BX-795 using three control fibroblast cell lines and six human NB cell lines. **(A)** Control fibroblast cell lines WI-38, NIH-3T3, COS-7. **(B)** MYCN amplified cell lines NGP, LAN-5, CHLA-255-MYCN. **(C)** MYCN non-amplified cell lines SH-SY-5Y, SK-N-AS, CHLA-255. **(D)** Summery table of IC50 values calculated for different cell lines as shown in A, B, and C. **(E and F)** Colony formation assay in response to BX-795 in NB cells. **(E)** Representative images of colony formation assay in response to BX-795 treatments. **(F)** Survival index showing relative colony number counts in response to BX-795 treatment. * $p < 0.05$; ** $p < 0.01$, *** $p < 0.001$.

tumors. These 3D models generate a solid anchorage-independent spheroid mass that closely mimics the *in vivo* growth of solid tumors. As shown in Fig. 5, similar size spheroids were developed, randomized, and subjected to increasing doses of BX-795. The size and growth of each spheroid was measured and imaged on day 0, 3, 5, and 7 (Fig. 5A, B). Results show a statistically significant and dose-dependent inhibition of NB spheroidal growth by BX-795 in comparison to control treatment (Fig. 5A, B). Additionally, fluorescence staining of day 7 terminal spheroids demonstrates a significant and dose-dependent reduction of live cells stained with calcein AM (green) and increase in dead cells stained with EthD-III (red) (Fig. 5C; and supplementary Fig. S2). These results were further confirmed by using a live cell ATP releasing assay which demonstrated that BX-795 significantly, and in a dose-dependent manner, induces tumor cell death inhibit NB spheroid growth (Fig. 5D).

BX-795 inhibits AKT pathway to suppress NB growth

BX-795 is known to directly inhibits PDK1 phosphorylation which in turn inhibits the AKT pathway [46]. Therefore, we performed RT-qPCR assays and Western blot assays to further elucidate the mechanism of action of BX-795 in NB. RT-qPCR assay results showed that BX-795 significantly inhibits the mRNA expression of PDK1, TBK1, AKT1, MTOR, and MYCN genes in a dose-dependent manner as compared to the controls (Fig. 6A). Additionally, Western blot analysis showed that BX-795 significantly inhibits total PDK1 levels as well as phosphorylation at its S241 catalytic site (Fig. 6B). As expected, we further observed significant inhibition of pAKT (T308) and pS6K (T389) levels in response to BX-795 treatments in a dose-dependent manner (Fig. 6B) in comparison total AKT and S6K. Overall, our molecular assays showed that BX-795 inhibits PDK1 at both the mRNA and protein levels, while also inhibiting PDK1 phosphorylation mediated activation, leading the overall inhibition of the oncogenic AKT pathway in NB.

BX-795 sensitizes NB to chemotherapy and crizotinib

We further planned to develop dual therapeutic approaches by combining BX-795 with either doxorubicin or crizotinib. Doxorubicin is a well-established chemotherapeutic drug and is regularly used in NB induction therapy regimens [47], while crizotinib is a multi-target ALK inhibitor currently in clinical trials for the treatment of NB [48]. Therefore, we combined BX-795 with doxorubicin and crizotinib to observe whether BX-795 can sensitizes NB by synergizing with these drugs. We utilized 4 NB cell lines, including 2 MYCN amplified NGP (ALK WT), LAN-5 (ALK R1275Q), and 2 MYCN non-amplified SK-N-AS (ALK WT), SH-SY5Y (ALK F1174L) for these experiments, and performed cell proliferation assays by treating NB cells with drug alone or in combination.

The Chou-Talalay method was used to determine the drug combination ratios and index [49]. BX-795 with doxorubicin and crizotinib were combined in equipotent ratios based on the IC50 values of single drugs. Results showed that both combinations, BX-795 + doxorubicin and BX-795 + crizotinib, act synergistically to significantly inhibit NB cell proliferation in comparison to any drug alone (Figs. 7A–D, 8A–D). Combining BX-795 with doxorubicin synergistically reduces the IC50 values of doxorubicin by 3.0- to 6.8-fold in NGP and SK-N-AS cell lines, respectively (Fig. 7A–D). Combining BX-795 with crizotinib only sensitizes ALK mutated cell lines SH-SY5Y (F1174L) and LAN-5 (R1275Q) but not the ALK wild type cell lines SK-N-AS and NGP (Fig. 8). BX-795 synergistically reduces the IC50 values of crizotinib by 15-fold in SH-SY5Y and 22-fold in LAN-5 cell lines, respectively (Fig. 8).

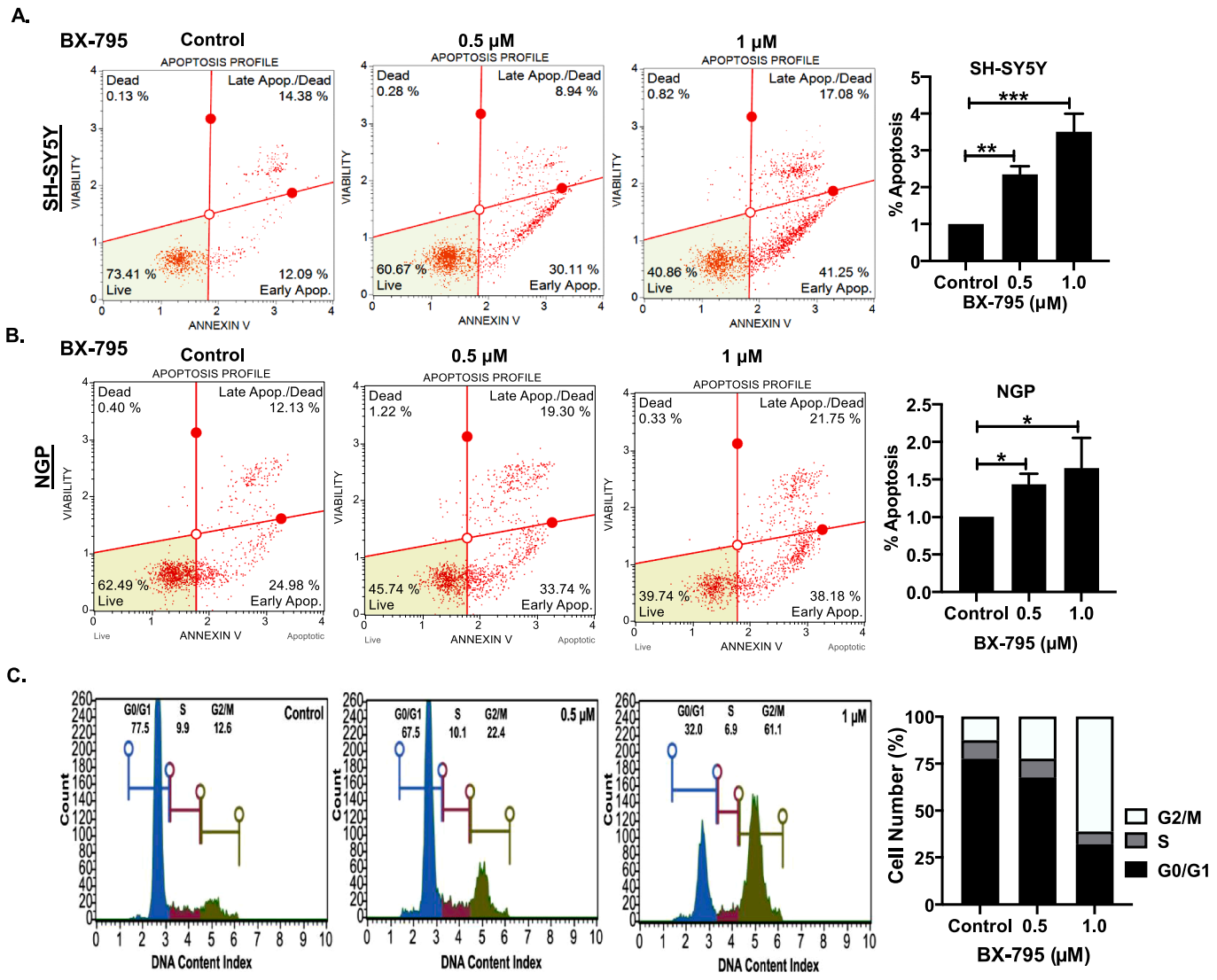

Fig. 4. *BX-795 induces apoptosis and blocks cell cycle progression in NB.* **(A, B)** Apoptosis assays in different NB cell lines in response to BX-795 treatments. **(A)** SH-SY5Y, **(B)** NGP. **(C)** Cell cycle analysis in NB SH-SY5Y cells. Representative images are shown. Percentage apoptosis displaying early apoptotic cells (A, B) and percentage cell number displaying cell cycle analysis (C) data for respective cell line in response to BX-795 treatments. * $p < 0.05$; ** $p < 0.01$, *** $p < 0.001$.

Dose-reduction indices (DRIs) plots indicated a favorable dose reduction with a DRI > 1 indicating favorable dose-reduction (Supplementary Fig. S3). The combination indexes (CI) were determined at the median effective doses 50 (ED50), ED75, ED90, and ED95 and found to be lower than 1.0 (CI< 1), indicating a synergistic effect between BX-795 and doxorubicin, and BX-795 and crizotinib in inhibiting NB growth (Figs. 7 and 8).

Furthermore, we evaluated the synergistic effects of BX-795 and doxorubicin in our NB 3D spheroid tumor model developed using the SH-SY5Y NB cell line. Similar sized spheroids were treated with either drug alone or in combination (Fig. 9). The results showed that combination of BX-795 with doxorubicin significantly inhibits 3D tumor spheroid growth in comparison to either drug alone (Fig. 9A, B). Additionally, combination cohorts showed significant inhibition of live tumor cells as determined by an ATP assay and staining with Calcein AM (Figs. 9C, D, and Supplementary S4). Similarly, and as expected, a significant increase was observed in the number of dead cells in combination treated cohorts as determined by staining with EthD-III (Supplementary Fig. S4C). Overall, our results showed that inhibiting the AKT pathway by BX-795 and further combining it with chemotherapy drug is a novel therapeutic approach for NB.

Discussion

PI3K/AKT signaling pathway involves numerous stimuli and plays an essential physiological role in maintaining cell homeostasis under normal conditions [50]. Studies have reported that PDK1 plays an essential role in various biological processes, including cell survival, proliferation, differentiation, migration, and cellular metabolism [51, 52]. The upregulation of PDK1 is mainly due to the catalytic activity of PIP3 driven by PI3K under normal physiological conditions [53]. Aberrant activation of the PI3K/AKT pathway is common in different types of cancers [50]. Blockage of the PDK1 activation can hinder cancer growth and metastasis by inhibiting the downstream AKT signaling cascade [50].

In the present study, we demonstrated that aberrant activation of AKT and related signaling pathway genes significantly alters the oncogenic potential of NB. The gene expression analysis of NB patients revealed that AKT1 and AKT2 strongly corelates with overall survival and disease progression. Patient dataset expression analysis also revealed that AKT1/2 strongly correlates with MYCN amplification and disease progression. Similar observations for multiple oncogenes were shown earlier in different studies using NB patient datasets [54, 55]. Studies have shown that inhibition of AKT expression inhibits tumor

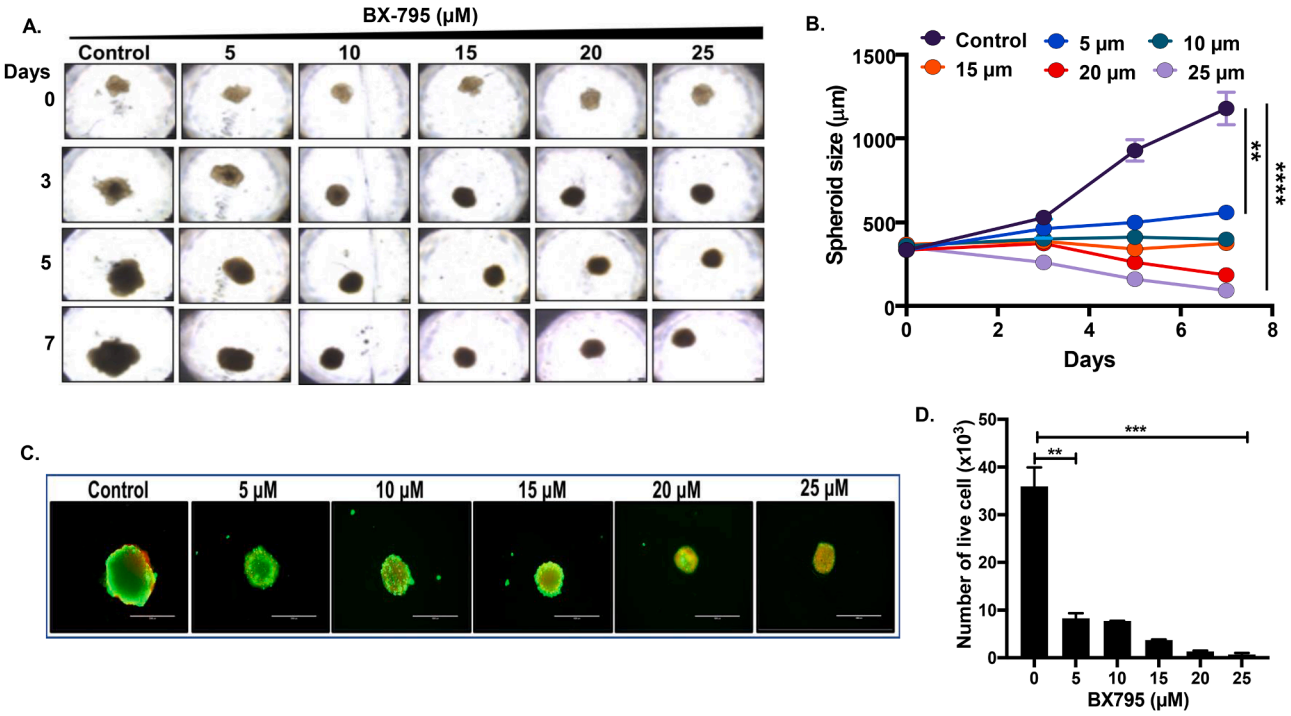

Fig. 5. *BX-795 inhibits NB spheroid tumor growth.* **(A)** Representative spheroid images at different days in response to BX-795 treatment. **(B)** Spheroid tumor growth as displayed in A. **(C)** Representative images of terminal spheroids at day 7 stained with Calcein AM and Ethidium homodimer III fluorescence dyes. **(D)** Quantitative measurement of number of live cells in terminal spheroids at day 7. * $p < 0.05$; ** $p < 0.01$, *** $p < 0.001$. Additional data in Supplementary Fig. S2.

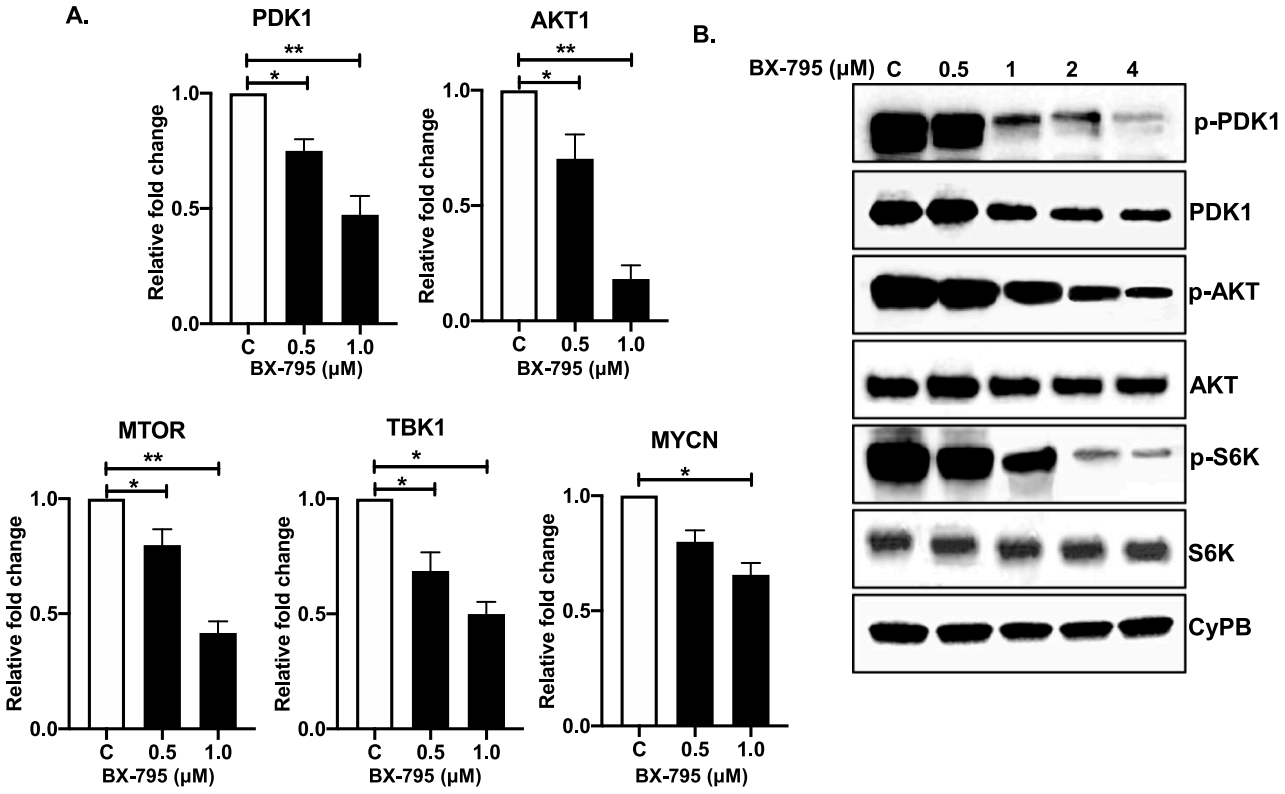

Fig. 6. *BX-795 inhibits AKT pathway*. **(A)** Gene expression analysis of PDK1, AKT1, MTOR, TBK1, and MYCN in response to BX-795 treatments in SH-SY5Y cells. **(B)** Western blot analysis of different AKT pathway proteins in response to increasing concentrations of BX-795 treatments. CyPB is used as loading control. * $p < 0.05$; ** $p < 0.01$.

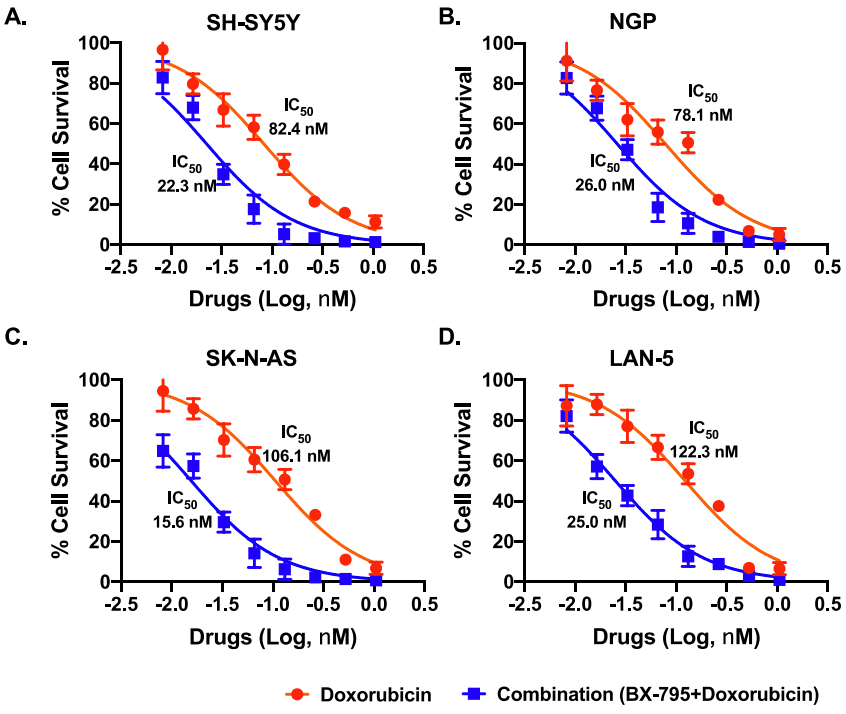

Fig. 7. *BX-795 synergizes NB to chemotherapy doxorubicin.* Combination index (CI) studies were performed by performing cell cytotoxicity assays in response to either doxorubicin alone or in combination with BX-795 in four NB cell lines at a ratio of 64:1. **(A)** SH-SY-5Y. **(B)** NGP. **(C)** SK-N-AS. **(D)** LAN-5. Cytotoxicity IC50 values are indicated next to corresponding treatment curves. **(E)** Summary of drug synergy values represented as combination index (CI). CI values for the combination of BX-795 and doxorubicin at different effective doses (ED50, ED75, ED90, ED95). CI values were calculated by the Chou-Talalay method for drug interactions. Values of CI < 1, $= 1$ and > 1 indicate synergism, additive effects, and antagonism, respectively.

E. Drug synergy study CI values

	Combination Index (CI)			
Cell line	ED50	ED75	ED90	ED95
SH-SY5Y	0.96131	0.69481	0.50262	0.40346
SK-N-AS	0.53514	0.39112	0.28602	0.23125
LAN-5	0.86761	0.79359	0.73945	0.71109
NGP	1.05721	0.83374	0.65789	0.56018

growth in different cancers, including NB [3,11,56].

Our results demonstrate the efficacy of BX-795 in inhibiting NB proliferation and induce cytotoxicity in a dose-dependent manner. Similar results were observed for an AKT inhibitor by blocking PDK1 and suppressing NB growth [13]. Therefore, to the best of our knowledge, this is the first report demonstrating the potency of BX-795 in NB. BX-795 is a small molecule inhibitor with an aminopyrimidine backbone in its chemical structure that acts as an ATP competitive inhibitor to target PDK1 phosphorylation and therefore inhibits AKT activation [14]. AKT has been an attractive target for treating different types of cancers, including NB. Previous studies reported that AKT inhibition reduces the proliferation of both MYCN amplified and MYCN non-amplified NB cells [11,57]. BX-795 has been shown to inhibit cancer cell proliferation and migration by inhibiting the TBK1 pathway in melanoma, bladder cancer, non-small cell lung cancer, oral squamous cell carcinoma (OSCC), colorectal cancer, and tamoxifen-resistant breast cancer [44,58,59]. These studies further validate our findings of the anti-proliferative effects of BX-795 in NB. BX-795 is also well-known for its anti-PDK1 activity and has also been shown to block GSK3β (Ser9) phosphorylation, another well-characterized target of the AKT pathway in prostate cancer cells [14]. Increasing evidence has shown that BX-795 is a suppressor of phosphorylation, nuclear translocation, and transcriptional activity of interferon regulatory factor 3 (IRF3), which further blocks interferon β production, but no effect on NFκB in Abelson murine leukemia virus cells [60]. In contrast, BX-795 has been reported to arrest the M phase of OSCC cells by down-regulating AKT and NFκB signaling pathway proteins [28]. These results are similar to our findings of BX-795 potently inducing apoptosis and blocking cell cycle progression at the mitotic phase in NB [61].

Our results also demonstrate that BX-795-mediated PDK1 inhibition was able to suppress NB proliferation and oncogenic potential, and this correlates with reduced levels of p-PDK1 (S241), p-AKT (Thr308), and p-S6K (Thr389). Therefore, our results established that PDK1-mediated AKT inhibition is a promising therapeutic strategy for NB. By inhibiting the phosphorylation of PDK1, BX-795 inhibits AKT activation and the overall downstream pathway, as shown by our Western blot analysis.

These results further motivate us to establish the potency of BX-795 in a NB tumor model, therefore we developed and utilized NB 3D spheroid models. The 3D tumor spheroid models have been shown to recapitulate the *in vivo* growth of solid tumors and became a gold standard to determine the drug effects in cancer cells by replacing expensive and time-consuming animal models [62–66]. Our spheroid tumor studies showed a dose-dependent tumor size reduction in response to BX-795. Previous research on tamoxifen resistant breast cancer showed tumor size reduction using *in vitro* tumor models.

ALK plays an important role in NB prognosis and around 7% of NB patients are ALK positive at diagnosis, while 20–22% of relapsed NB patients are ALK positive, regardless of initial ALK status [48,67]. Current NB therapies include surgery, radiation, and induction chemotherapy approaches either alone or combined. These therapeutic approaches are highly genotoxic and induce severe side-effects including secondary cancers in patients [68,69]. Therefore, it is important to develop less-toxic and more-effective therapeutic approaches for NB. With this goal, we sought to combine BX-795 with

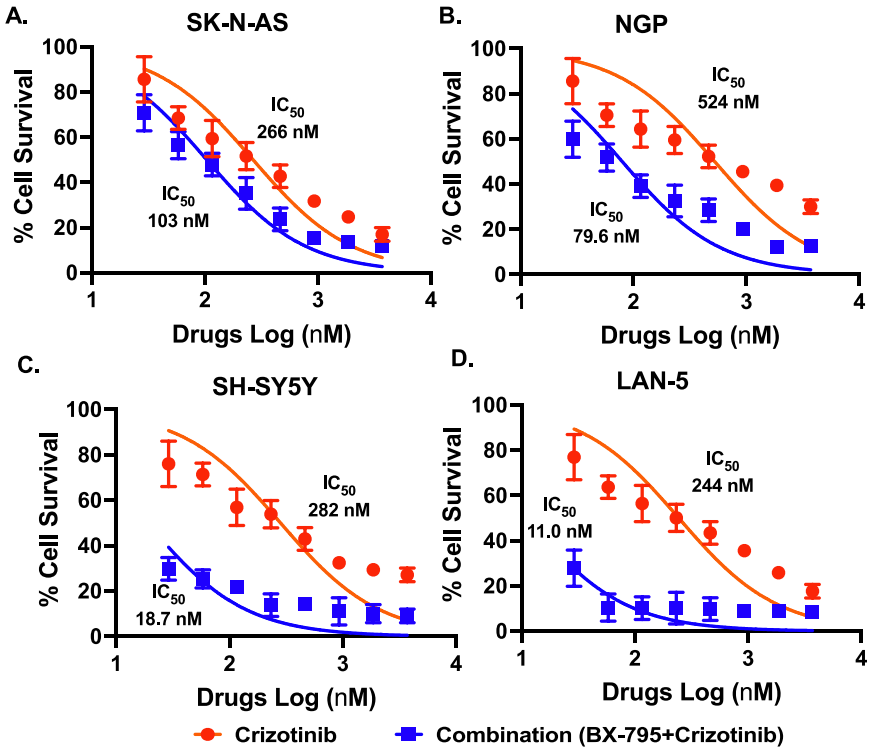

Fig. 8. *BX-795 synergizes NB to ALK inhibitor crizotinib.* Combination index (CI) studies were performed by performing cell cytotoxicity assays in response to either crizotinib alone or in combination with BX-795 in four NB cell lines. **(A)** SK-N-AS. **(B)** NGP. **(C)** SH-SY5Y. **(D)** LAN-5. Cytotoxicity IC50 values are indicated next to corresponding treatment curves. **(E)** Summary of drug synergy values represented as combination index (CI). CI values for the combination of BX-795 and crizotinib at different effective doses (ED50, ED75, ED90, ED95).

E.

		Combination Index (CI)			
	Cell line	ED50	ED75	ED90	ED95
ALK status: Mutated	SH-SY5Y	0.08735	0.12310	0.20947	0.50105
	LAN-5	0.20869	0.28645	0.39467	0.49318
WT	SK-N-AS	6.19935	7.25325	8.50386	9.49664
	NGP	1.60295	2.77915	4.84000	7.09752

chemotherapy drugs, such as doxorubicin and crizotinib. Our results demonstrate that BX-795 synergizes NB to chemotherapy doxorubicin and potently inhibits NB growth in both 2D proliferation assays and 3D tumor spheroid model. We also observed BX-795 significantly synergizes crizotinib to ALK mutated NB cell line SH-SY5Y (F1174L) and LAN-5 (R1275Q) in contrast ALK wild type NB cell lines. Similar results were reported earlier for combining crizotinib with an ATP-competitive mTOR inhibitor Torin 2 [70,71]. Crizotinib sensitizes ALK mutated NB cells to Torin 2 in both *in vitro* and *in vivo* models.

Overall, our study clearly demonstrates the potency of BX-795 in inhibiting NB growth by directly targeting PDK1 activation to inhibit the AKT pathway. BX-795 induces apoptosis and block cell cycle progression in NB. Our study also highlights the efficacy of BX-795 in sensitizing NB to current therapies, and further developing dual therapeutic approaches for NB.

Funding support

This work is funded by the Scholar Career Development Award from the St. Baldrick's Foundation, and Seed grant from the St. John's University to Dr. Saurabh Agarwal. RC, DR., and AK are supported by the Graduate Teaching Assistantships from the St. John's University.

CRediT authorship contribution statement

Rameswari Chilamakuri: Methodology, Validation, Investigation, Writing – original draft, Writing – review & editing, Visualization. **Danielle C. Rouse:** Methodology, Investigation. **Yang Yu:** Methodology, Investigation. **Abbas S. Kabir:** Methodology. **Aaron Muth:** Writing – original draft, Writing – review & editing, Resources. **Jianhua Yang:** Validation, Investigation, Resources. **Jeffery M. Lipton:** Validation, Investigation, Resources. **Saurabh Agarwal:** Conceptualization, Methodology, Investigation, Writing – original draft, Writing – review & editing, Visualization, Supervision, Project administration, Funding acquisition.

CRediT authorship contribution statement

Rameswari Chilamakuri: Methodology, Validation, Investigation, Writing – original draft, Writing – review & editing, Visualization. **Danielle C. Rouse:** Methodology, Investigation. **Yang Yu:** Methodology, Investigation. **Abbas S. Kabir:** Methodology. **Aaron Muth:** Writing – original draft, Writing – review & editing, Resources. **Jianhua Yang:** Validation, Investigation, Resources. **Jeffery M. Lipton:** Validation, Investigation, Resources. **Saurabh Agarwal:** Conceptualization, Methodology, Investigation, Writing – original draft, Writing – review & editing, Visualization, Supervision, Project administration, Funding acquisition.

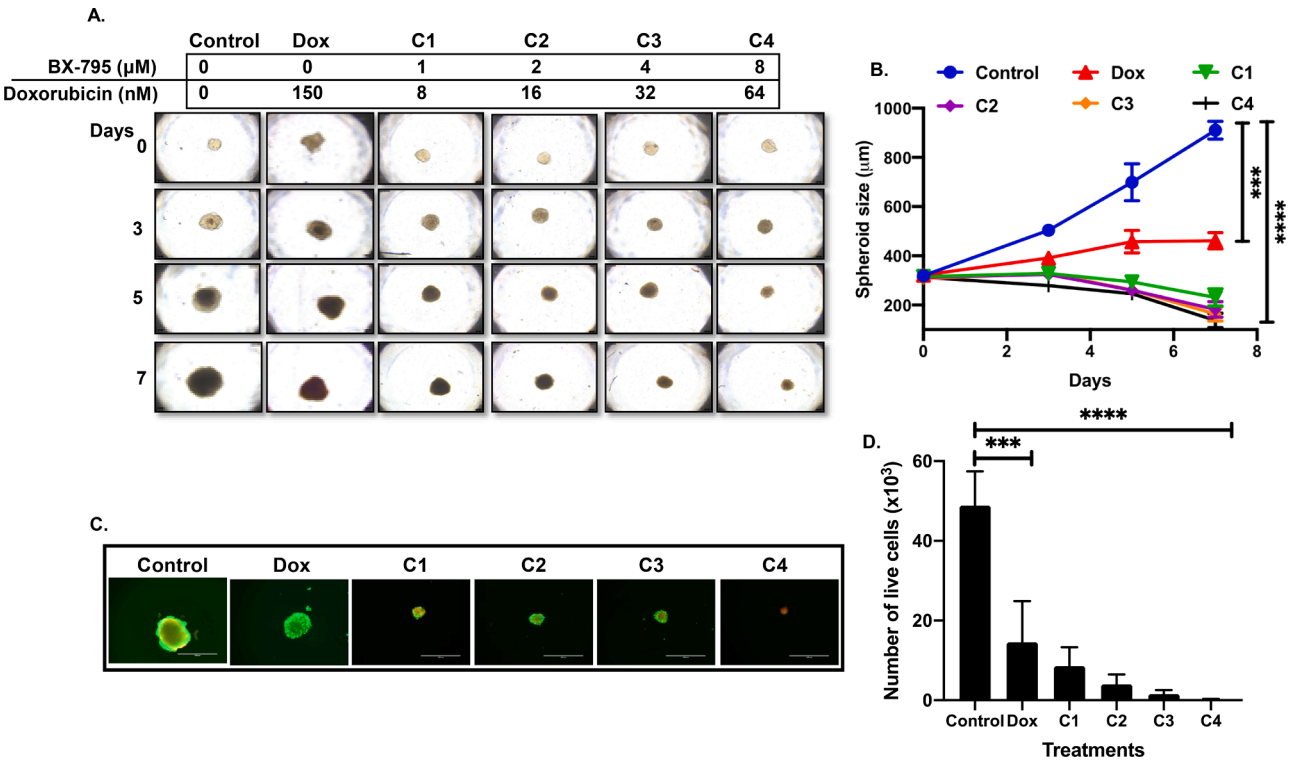

Fig. 9. *Combination therapy synergistically reduces NB spheroid tumor growth.* 3D spheroid tumors were treated with either doxorubicin alone or in combination with BX-795 at indicated doses. **(A)** Representative images of 3D spheroid tumors showing synergistic reduction in tumor mass. **(B)** Spheroid tumor mass measurements at different days during treatment. **(C)** Representative images of terminal spheroids at day 7 stained with Calcein AM and Ethidium homodimer III fluorescence dyes. **(D)** Quantitative measurement of number of live cells in terminal spheroids at day 7. *** $p < 0.001$, **** $p < 0.0001$. Additional data in Supplementary Fig. S3.

Declaration of Competing Interest

The authors declare that they have no known competing financial interests or personal relationships that could have appeared to influence the work reported in this paper.

Supplementary materials

Supplementary data associated with this article can be found, in the online version, at doi:10.1016/j.tranon.2021.101272.

References

[1] J.A. Tomolonis, S. Agarwal, J.M. Shohet, Neuroblastoma pathogenesis: deregulation of embryonic neural crest development, Cell Tissue Res. 372 (2018) 245–262.
[2] V. Smith, J. Foster, High-risk neuroblastoma treatment review, Child. (Basel) 5 (2018).
[3] N. Jiang, Q. Dai, X. Su, J. Fu, X. Feng, J. Peng, Role of PI3K/AKT pathway in cancer: the framework of malignant behavior, Mol. Biol. Rep. 47 (2020) 4587–4629.
[4] M.S. Song, L. Salmena, P.P. Pandolfi, The functions and regulation of the PTEN tumour suppressor, Nat. Rev. Mol. Cell Biol. 13 (2012) 283–296.
[5] B. Ananthanarayanan, Q. Ni, J. Zhang, Signal propagation from membrane messengers to nuclear effectors revealed by reporters of phosphoinositide dynamics and Akt activity, Proc. Natl. Acad. Sci. U. S. A. 102 (2005) 15081–15086.
[6] M. Laplante, D.M. Sabatini, mTOR signaling in growth control and disease, Cell 149 (2012) 274–293.
[7] B.Y. Shorning, M.S. Dass, M.J. Smalley, H.B. Pearson, The PI3K-AKT-mTOR pathway and prostate cancer: at the crossroads of AR, MAPK, and WNT signaling, Int. J. Mol. Sci. 21 (2020).
[8] Q. Chen, M. Wang, C. Shen, Bauerane induces S-phase cell cycle arrest, apoptosis, and inhibition of proliferation of A549 human lung cancer cells through the phosphoinositide 3-kinase (PI3K)/AKT and signal transducer and activator of transcription 3 (STAT3) signaling pathway, Med. Sci. Monit. 26 (2020), e919558.
[9] A. Zaczek, P. Jozwiak, P. Ciesielski, E. Forma, K. Wojcik-Krowiranda, L. Cwonda, A. Bienkiewicz, M. Brys, A. Krzeslak, Relationship between polycomb-group protein BMI-1 and phosphatases regulating AKT phosphorylation level in endometrial cancer, J. Cell Mol. Med. 24 (2020) 1300–1310.
[10] J. Ma, H. Wang, S. Guo, X. Yi, T. Zhao, Y. Liu, Q. Shi, T. Gao, C. Li, W. Guo, A20 promotes melanoma progression via the activation of Akt pathway, Cell Death Dis. 11 (2020) 794.
[11] D. Opel, C. Poremba, T. Simon, K.M. Debatin, S. Fulda, Activation of Akt predicts poor outcome in neuroblastoma, Cancer Res. 67 (2007) 735–745.
[12] X. Yu, H. Fan, X. Jiang, W. Zheng, Y. Yang, M. Jin, X. Ma, W. Jiang, Apatinib induces apoptosis and autophagy via the PI3K/AKT/mTOR and MAPK/ERK signaling pathways in neuroblastoma, Oncol. Lett. 20 (2020) 52.
[13] J. Navratilova, M. Karasova, M. Kohutkova Lanova, L. Jirakova, Z. Budkova, J. Pachernik, J. Smarda, P. Benes, Selective elimination of neuroblastoma cells by synergistic effect of Akt kinase inhibitor and tetrathiomolybdate, J. Cell Mol. Med. 21 (2017) 1859–1869.
[14] G. Nalairndran, A. Hassan Abdul Razack, C.W. Mai, F.Fei-Lei Chung, K.K. Chan, L. W. Hii, W.M. Lim, I. Chung, C.O. Leong, Phosphoinositide-dependent Kinase-1 (PDPK1) regulates serum/glucocorticoid-regulated Kinase 3 (SGK3) for prostate cancer cell survival, J. Cell Mol. Med. 24 (2020) 12188–12198.
[15] M. Hetman, J.E. Cavanaugh, D. Kimelman, Z. Xia, Role of glycogen synthase kinase-3beta in neuronal apoptosis induced by trophic withdrawal, J. Neurosci. 20 (2000) 2567–2574.
[16] N. Balasuriya, N.E. Davey, J.L. Johnson, H. Liu, K.K. Biggar, L.C. Cantley, S.S. Li, P. O'Donoghue, Phosphorylation-dependent substrate selectivity of protein kinase B (AKT1), J. Biol. Chem. 295 (2020) 8120–8134.
[17] A. Emmanouilidi, M. Falasca, Targeting PDK1 for chemosensitization of cancer cells, Cancers (Basel) 9 (2017).
[18] Y. Zhou, Y. Li, S. Xu, J. Lu, Z. Zhu, S. Chen, Y. Tan, P. He, J. Xu, C.G. Proud, J. Xie, K. Shen, Eukaryotic elongation factor 2 kinase promotes angiogenesis in hepatocellular carcinoma via PI3K/Akt and STAT3, Int. J. Cancer 146 (2020) 1383–1395.
[19] Y. Wang, D. Zhang, Y. Li, F. Fang, MiR-138 suppresses the PDK1 expression to decrease the oxaliplatin resistance of colorectal cancer, Onco Targets Ther. 13 (2020) 3607–3618.
[20] J. Qin, M. Fu, J. Wang, F. Huang, H. Liu, M. Huangfu, D. Yu, H. Liu, X. Li, X. Guan, X. Chen, PTEN/AKT/mTOR signaling mediates anticancer effects of epigallocatechin3gallate in ovarian cancer, Oncol. Rep. 43 (2020) 1885–1896.
[21] H. Lu, Y. Lu, Y. Xie, S. Qiu, X. Li, Z. Fan, Rational combination with PDK1 inhibition overcomes cetuximab resistance in head and neck squamous cell carcinoma, JCI Insight 4 (2019).
[22] L.U. Li, Y. Zhao, H. Zhang, P16INK4a upregulation mediated by TBK1 induces retinal ganglion cell senescence in ischemic injury, Cell Death Dis. 8 (2017) e2752.
[23] R.I. Feldman, J.M. Wu, M.A. Polokoff, M.J. Kochanny, H. Dinter, D. Zhu, S.L. Biroc, B. Alicke, J. Bryant, S. Yuan, B.O. Buckman, D. Lentz, M. Ferrer, M. Whitlow, M. Adler, S. Finster, Z. Chang, D.O. Arnaiz, Novel small molecule inhibitors of 3-phosphoinositide-dependent kinase-1, J. Biol. Chem. 280 (2005) 19867–19874.

[24] S. Xiang, S. Song, H. Tang, J.B. Smaill, A. Wang, H. Xie, X. Lu, TANK-binding kinase 1 (TBK1): an emerging therapeutic target for drug discovery, Drug Discov. Today (2021).
[25] D. Jaishankar, A.M. Yakoub, T. Yadavalli, A. Agelidis, N. Thakkar, S. Hadigal, J. Ames, D. Shukla, An off-target effect of BX795 blocks herpes simplex virus type 1 infection of the eye, Sci. Transl. Med. 10 (2018).
[26] A. Iqbal, R. Suryawanshi, T. Yadavalli, I. Volety, D. Shukla, BX795 demonstrates potent antiviral benefits against herpes simplex Virus-1 infection of human cell lines, Antiviral Res. 180 (2020), 104814.
[27] T. Yu, Z. Wang, W. Jie, X. Fu, B. Li, H. Xu, Y. Liu, M. Li, E. Kim, Y. Yang, J.Y. Cho, The kinase inhibitor BX795 suppresses the inflammatory response via multiple kinases, Biochem. Pharmacol. 174 (2020), 113797.
[28] L.Y. Bai, C.F. Chiu, N.P. Kapuriya, T.M. Shieh, Y.C. Tsai, C.Y. Wu, A.M. Sargeant, J. R. Weng, BX795, a TBK1 inhibitor, exhibits antitumor activity in human oral squamous cell carcinoma through apoptosis induction and mitotic phase arrest, Eur. J. Pharmacol. 769 (2015) 287–296.
[29] M. Mokou, V. Lygirou, I. Angelioudaki, N. Paschalidis, R. Stroggilos, M. Frantzi, A. Latosinska, A. Bamias, M.J. Hoffmann, H. Mischak, A. Vlahou, A novel pipeline for drug repurposing for bladder cancer based on patients' Omics signatures, Cancers (Basel) 12 (2020).
[30] W. Chen, K. Luo, Z. Ke, B. Kuai, S. He, W. Jiang, W. Huang, Z. Cai, TBK1 promote bladder cancer cell proliferation and migration via Akt signaling, J. Cancer 8 (2017) 1892–1899.
[31] E.A. Choi, Y.S. Choi, E.J. Lee, S.R. Singh, S.C. Kim, S. Chang, A pharmacogenomic analysis using L1000CDS(2) identifies BX-795 as a potential anticancer drug for primary pancreatic ductal adenocarcinoma cells, Cancer Lett. 465 (2019) 82–93.
[32] C. Wei, Y. Cao, X. Yang, Z. Zheng, K. Guan, Q. Wang, Y. Tai, Y. Zhang, S. Ma, Y. Cao, X. Ge, C. Xu, J. Li, H. Yan, Y. Ling, T. Song, L. Zhu, B. Zhang, Q. Xu, C. Hu, X.W. Bian, X. He, H. Zhong, Elevated expression of TANK-binding kinase 1 enhances tamoxifen resistance in breast cancer, Proc. Natl. Acad. Sci. U. S. A. 111 (2014) E601–E610.
[33] O.A. Bamodu, H.L. Chang, J.R. Ong, W.H. Lee, C.T. Yeh, J.T. Tsai, Elevated PDK1 expression drives PI3K/AKT/MTOR signaling promotes radiation-resistant and dedifferentiated phenotype of hepatocellular carcinoma, Cells 9 (2020).
[34] H. Huang, Anaplastic lymphoma kinase (ALK) receptor tyrosine kinase: a catalytic receptor with many faces, Int. J. Mol. Sci. 19 (2018).
[35] R.M. Trigg, S.D. Turner, ALK in neuroblastoma: biological and therapeutic implications, Cancers (Basel) 10 (2018).
[36] H. Huang, A. Gont, L. Kee, R. Dries, K. Pfeifer, B. Sharma, D.N. Debruyne, M. Harlow, S. Sengupta, J. Guan, C.M. Yeung, W. Wang, B. Hallberg, R.H. Palmer, M.S. Irwin, R.E. George, Extracellular domain shedding of the ALK receptor mediates neuroblastoma cell migration, Cell Rep. 36 (2021), 109363.
[37] R. Versteeg, R.E. George, Targeting ALK: the ten lives of a tumor, Cancer Discov. 6 (2016) 20–21.
[38] J. Muranyi, A. Varga, P. Gyulavari, K. Penzes, C.E. Nemeth, M. Csala, L. Petho, A. Csampai, G. Halmos, I. Petak, I. Valyi-Nagy, Novel crizotinib-GnRH conjugates revealed the significance of lysosomal trapping in GnRH-based drug delivery systems, Int. J. Mol. Sci. 20 (2019).
[39] L. Li, Y. Wang, T. Peng, K. Zhang, C. Lin, R. Han, C. Lu, Y. He, Metformin restores crizotinib sensitivity in crizotinib-resistant human lung cancer cells through inhibition of IGF1-R signaling pathway, Oncotarget 7 (2016) 34442–34452.
[40] S. Agarwal, A. Lakoma, Z. Chen, J. Hicks, L.S. Metelitsa, E.S. Kim, J.M. Shohet, G-CSF promotes neuroblastoma tumorigenicity and metastasis via STAT3-dependent cancer stem cell activation, Cancer Res. 75 (2015) 2566–2579.
[41] S. Agarwal, R. Ghosh, Z. Chen, A. Lakoma, P.H. Gunaratne, E.S. Kim, J.M. Shohet, Transmembrane adaptor protein PAG1 is a novel tumor suppressor in neuroblastoma, Oncotarget 7 (2016) 24018–24026.
[42] H. Li, Y. Yu, Y. Zhao, D. Wu, X. Yu, J. Lu, Z. Chen, H. Zhang, Y. Hu, Y. Zhai, J. Su, A. Aheman, A. De Las Casas, J. Jin, X. Xu, Z. Shi, S.E. Woodfield, S.A. Vasudevan, S. Agarwal, Y. Yan, J. Yang, J.H. Foster, Small molecule inhibitor agerafenib effectively suppresses neuroblastoma tumor growth in mouse models via inhibiting ERK MAPK signaling, Cancer Lett. 457 (2019) 129–141.
[43] S. Guan, J. Lu, Y. Zhao, Y. Yu, H. Li, Z. Chen, Z. Shi, H. Liang, M. Wang, K. Guo, X. Chen, W. Sun, S. Bieerkehazhi, X. Xu, S. Sun, S. Agarwal, J. Yang, MELK is a novel therapeutic target in high-risk neuroblastoma, Oncotarget 9 (2018) 2591–2602.
[44] S. Agarwal, G. Milazzo, K. Rajapakshe, R. Bernardi, Z. Chen, E. Barbieri, J. Koster, G. Perini, C. Coarfa, J.M. Shohet, MYCN acts as a direct co-regulator of p53 in MYCN amplified neuroblastoma, Oncotarget 9 (2018) 20323–20338.
[45] J.C. Ashton, Drug combination studies and their synergy quantification using the Chou-Talalay method-letter, Cancer Res. 75 (2015) 2400.
[46] K. Clark, L. Plater, M. Peggie, P. Cohen, Use of the pharmacological inhibitor BX795 to study the regulation and physiological roles of TBK1 and IkappaB kinase epsilon: a distinct upstream kinase mediates Ser-172 phosphorylation and activation, J. Biol. Chem. 284 (2009) 14136–14146.
[47] C.U. Louis, J.M. Shohet, Neuroblastoma: molecular pathogenesis and therapy, Annu. Rev. Med. 66 (2015) 49–63.
[48] G. Umapathy, P. Mendoza-Garcia, B. Hallberg, R.H. Palmer, Targeting anaplastic lymphoma kinase in neuroblastoma, APMIS 127 (2019) 288–302.
[49] T.C. Chou, Drug combination studies and their synergy quantification using the Chou-Talalay method, Cancer Res. 70 (2010) 440–446.
[50] G. Hoxhaj, B.D. Manning, The PI3K-AKT network at the interface of oncogenic signalling and cancer metabolism, Nat. Rev. Cancer 20 (2020) 74–88.
[51] Y. Wei, X. Han, C. Zhao, PDK1 regulates the survival of the developing cortical interneurons, Mol. Brain 13 (2020) 65.
[52] R. Ichikawa, R. Kawasaki, A. Iwata, S. Otani, E. Nishio, H. Nomura, T. Fujii, MicroRNA1263p suppresses HeLa cell proliferation, migration and invasion, and increases apoptosis via the PI3K/PDK1/AKT pathway, Oncol. Rep. 43 (2020) 1300–1308.
[53] S. Darici, H. Alkhaldi, G. Horne, H.G. Jorgensen, S. Marmiroli, X. Huang, Targeting PI3K/Akt/mTOR in AML: rationale and clinical evidence, J. Clin. Med. 9 (2020).
[54] A. Villasante, A. Godier-Furnemont, A. Hernandez-Barranco, J.L. Coq, J. Boskovic, H. Peinado, J. Mora, J. Samitier, G. Vunjak-Novakovic, Horizontal transfer of the stemness-related markers EZH2 and GLI1 by neuroblastoma-derived extracellular vesicles in stromal cells, Transl. Res. (2021).
[55] F. Schmitt-Hoffner, S. van Rijn, U.H. Toprak, M. Mauermann, F. Rosemann, A. Heit-Mondrzyk, J.M. Hubner, A. Camgoz, S. Hartlieb, S.M. Pfister, K.O. Henrich, F. Westermann, M. Kool, FOXR2 stabilizes MYCN protein and identifies Non-MYCN-amplified neuroblastoma patients with unfavorable outcome, J. Clin. Oncol. (2021), JCO2002540.
[56] L. Qi, H. Toyoda, D.Q. Xu, Y. Zhou, N. Sakurai, K. Amano, K. Kihira, H. Hori, E. Azuma, Y. Komada, PDK1-mTOR signaling pathway inhibitors reduce cell proliferation in MK2206 resistant neuroblastoma cells, Cancer Cell Int. 15 (2015) 91.
[57] L. Segerstrom, N. Baryawno, B. Sveinbjornsson, M. Wickstrom, L. Elfman, P. Kogner, J.I. Johnsen, Effects of small molecule inhibitors of PI3K/Akt/mTOR signaling on neuroblastoma growth *in vitro* and *in vivo*, Int. J. Cancer 129 (2011) 2958–2965.
[58] F. Eduati, V. Doldan-Martelli, B. Klinger, T. Cokelaer, A. Sieber, F. Kogera, M. Dorel, M.J. Garnett, N. Bluthgen, J. Saez-Rodriguez, Drug resistance mechanisms in colorectal cancer dissected with cell type-specific dynamic logic models, Cancer Res. 77 (2017) 3364–3375.
[59] H.L. Vu, A.E. Aplin, Targeting TBK1 inhibits migration and resistance to MEK inhibitors in mutant NRAS melanoma, Mol. Cancer Res. 12 (2014) 1509–1519.
[60] S. Hobbs, M. Reynoso, A.V. Geddis, A.Y. Mitrophanov, R.W. Matheny, LPS-stimulated NF-kappaB p65 dynamic response marks the initiation of TNF expression and transition to IL-10 expression in RAW 264.7 macrophages, Physiol. Rep. 6 (2018) e13914.
[61] R. Gomez-Villafuertes, P. Garcia-Huerta, J.I. Diaz-Hernandez, M.T. Miras-Portugal, PI3K/Akt signaling pathway triggers P2X7 receptor expression as a pro-survival factor of neuroblastoma cells under limiting growth conditions, Sci. Rep. 5 (2015) 18417.
[62] S. Daunys, A. Janoniene, I. Januskeviciene, M. Paskeviciute, V. Petrikaite, 3D tumor spheroid models for *in vitro* therapeutic screening of nanoparticles, Adv. Exp. Med. Biol. 1295 (2021) 243–270.
[63] B.W. Huang, J.Q. Gao, Application of 3D cultured multicellular spheroid tumor models in tumor-targeted drug delivery system research, J. Control Release 270 (2018) 246–259.
[64] T.P. Raposo, S. Susanti, M. Ilyas, Investigating TNS4 in the colorectal tumor microenvironment using 3D spheroid models of invasion, Adv. Biosyst. 4 (2020), e2000031.
[65] M. Zanoni, F. Piccinini, C. Arienti, A. Zamagni, S. Santi, R. Polico, A. Bevilacqua, A. Tesei, 3D tumor spheroid models for *in vitro* therapeutic screening: a systematic approach to enhance the biological relevance of data obtained, Sci. Rep. 6 (2016) 19103.
[66] M. Zraikat, T. Alshelleh, Comparison between different 3D spheroid tumor invasion models, Assay Drug Dev. Technol. 18 (2020) 239–242.
[67] A.K. Brenner, M.W. Gunnes, Therapeutic targeting of the anaplastic lymphoma kinase (ALK) in neuroblastoma-a comprehensive update, Pharmaceutics 13 (2021).
[68] J.M. Maris, Recent advances in neuroblastoma, N. Engl. J. Med. 362 (2010) 2202–2211.
[69] S.B. Whittle, V. Smith, E. Doherty, S. Zhao, S. McCarty, P.E. Zage, Overview and recent advances in the treatment of neuroblastoma, Expert Rev. Anticancer Ther. 17 (2017) 369–386.
[70] T. Berry, W. Luther, N. Bhatnagar, Y. Jamin, E. Poon, T. Sanda, D. Pei, B. Sharma, W.R. Vetharoy, A. Hallsworth, Z. Ahmad, K. Barker, L. Moreau, H. Webber, W. Wang, Q. Liu, A. Perez-Atayde, S. Rodig, N.K. Cheung, F. Raynaud, B. Hallberg, S.P. Robinson, N.S. Gray, A.D. Pearson, S.A. Eccles, L. Chesler, R.E. George, The ALK(F1174L) mutation potentiates the oncogenic activity of MYCN in neuroblastoma, Cancer Cell 22 (2012) 117–130.
[71] N.F. Moore, A.M. Azarova, N. Bhatnagar, K.N. Ross, L.E. Drake, S. Frumm, Q.S. Liu, A.L. Christie, T. Sanda, L. Chesler, A.L. Kung, N.S. Gray, K. Stegmaier, R.E. George, Molecular rationale for the use of PI3K/AKT/mTOR pathway inhibitors in combination with crizotinib in ALK-mutated neuroblastoma, Oncotarget 5 (2014) 8737–8749.